Journal of
Nanoscience and Nanotechnology
Vol. 8, 6598–6602, 2008

Studies of Point Defect Formation and Self-Compensation in Indium Doped ZnO Nanorods by STM and STS

A. González-Carrazco[1], M. Herrera-Zaldívar[1,*], and U. Pal[2]

[1] *Centro de Ciencias de la Materia Condensada, Universidad Nacional Autónoma de México, Apdo. Postal 2681, C.P. 22800, Ensenada, Baja California, México*
[2] *Instituto de Física, Universidad Autónoma de Puebla, Apdo. Postal J-48, Puebla, Pue. 72570, México*

The effect of indium doping on the point defect formation in ZnO nanostructures is studied by scanning tunneling microscopy (STM) and scanning tunneling spectroscopy (STS) techniques. While the incorporation of a donor dopant like indium should increase the *n*-type conductivity of ZnO nanostructures, it has been found that formation of V_{Zn} native acceptors in heavily doped ZnO nanostructures produces self-compensation effect, creating acceptor states in their band gap. Presence of both donor and acceptor states in heavily indium doped ZnO nanostructures are probed and identified. The mechanism of formation of such donor and acceptor states is discussed.

Keywords: Scanning Tunneling Microscopy, Indium-Doped ZnO, Nanostructures, Self-Compensation, Point Defects.

1. INTRODUCTION

Synthesis and characterization of ZnO nanostructures are of great interest due to their potential applications in the fabrication of optoelectronic devices, such as highly efficient blue lasers and light-emitting diodes.[1] Due to its wide direct band gap (3.4 eV) and large exciton binding energy (60 meV), ZnO is one of the most important functional oxides, exhibiting near UV emission[2] and piezoelectricity,[3] and a promising material for sensing,[4] field emission and other optoelectronic applications.[5] Recently ZnO nanostructures of various geometries have been produced[6] using high[7,8] and low temperature synthesis techniques,[9,10] While the production of nanostructures with a particular morphology and desired electronic properties is of great interest for the material scientists, a better understanding of defect formation in them is essential for successful technological applications. The self-compensation effect in *n*-type ZnO, for example, is the subject of intense interest as it hinders the design of several optoelectronic devices.[11]

In wide band gap II–VI semiconductors of *n*-type conductivity, apparently it is impossible to convert *p*-type by incorporation of acceptor impurities at thermal equilibrium conditions due to generation of donor type native defects.[12] On the other hand, incorporation of donors in excess in *n*-type wide band gap semiconductor may produce defects which may form donor-defect complexes, metal atom vacancies (through substitution at lattice sites), and nonmetallic interstitial sites, preventing the effective incorporation of donor dopants. Formation of acceptor carriers could be an electrical response to high density of extrinsic donor carriers in ZnO, introducing defect states that favor the formation of parasitic emissions, such as the yellow and red emissions related to native O_i.[13,14]

In the present work, scanning tunneling microscopy (STM) and scanning tunneling spectroscopy (STS) techniques are used to show the evidences of self-compensation in nominally pure ZnO nanostructures by incorporating indium heavily. Apart from the donor defect states, formation of acceptor-like native defects in heavily indium doped ZnO nanostructures are identified and discussed.

2. EXPERIMENTAL DETAILS

Undoped and indium doped ZnO nanorods were synthesized using a low temperature hydrothermal process as reported earlier.[15] In a typical synthesis process, 10.25 g of zinc acetate dihydrate ($Zn(CH_3COO)_2 \cdot 2H_2O$; Aldrich, 99.99%) was added to 120 ml of aqueous solution of ethylenediamine (10% volume, $NH_2(CH_2)_2NH_2$; Baker, 99.9%), followed by the addition of 1.70 g of sodium hydroxide (NaOH; Aldrich, 99.99%) under agitation. The mixture solution was heated in a round bottom flask at

*Author to whom correspondence should be addressed.

 1533-4880/2008/8/6598/005 doi:10.1166/jnn.2008.035

90 °C for 15 h. After cooling to room temperature, the product was washed and dried at 80 °C for 2 h. For doping, a nominal 2 mole% of indium chloride ($InCl_3$; Aldrich, 99.999%) was added to the reaction mixture before heating.

For STM observations, a drop of the powder sample previously dispersed in water was deposited on a gold coated glass surface and dried at room temperature. The nanorods were observed using a JEOL JSM5300 scanning electron microscope (SEM) with attached Noran SuperDry analytical system, and a NanoScope E scanning tunneling microscope (STM; Digital Instruments) operating at room temperature and in air. All the STM images presented in this work were taken in constant current mode, using electrochemically etched W wires or mechanically sharpened Pt-Ir wires as probe tips. With scanning tunneling spectroscopy (STS), the occupied and unoccupied states can be probed by monitoring the tunnel current when the sample is negatively and positively biased, respectively. In our study, I–V data were collected in spectroscopy mode following a common procedure: the feedback loop of the microscope that controls the vertical motion of the tip was interrupted for 0.3 ms and the bias voltage was digitally ramped from an initial to final pre-selected values, while the corresponding tunnel current was digitally sampled. STS measurements were made by averaging 6–8 current–voltage curves at various locations on individual nanorods. The normalized differential conductance spectra presented as the ratio $(dI/dV)/(I/V)$, give a direct measure of the surface density of states of the samples.[16, 17]

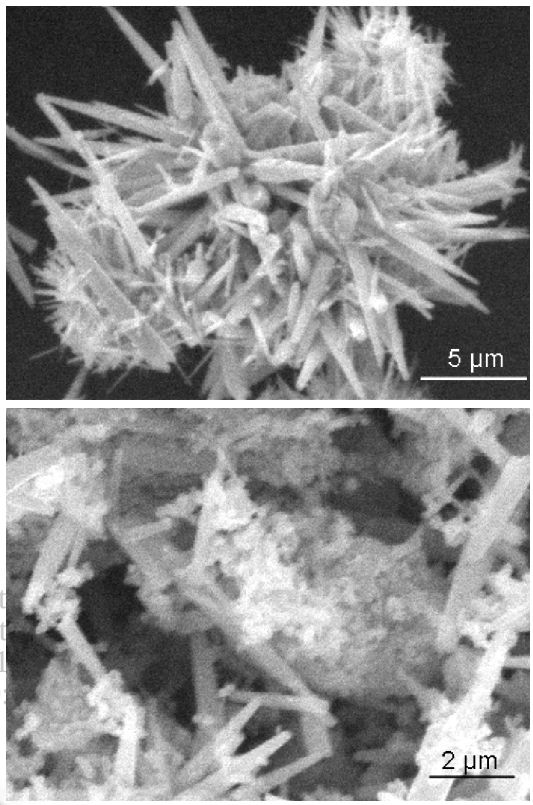

Fig. 1. Secondary electron images of (a) undoped, and (b) In doped (2%) ZnO nanorods. Formation of nanoparticles over ZnO nanorods can be seen in the latter sample.

3. RESULTS AND DISCUSSION

Typical secondary electron images of the undoped and indium doped ZnO nanorods are shown in Figure 1. While the undoped sample revealed conical shaped nanorods of about 420 nm average diameters and about 5.5 μm of average length (Fig. 1(a)), the doped sample revealed similar nanorods along with numerous nanoparticles that occasionally appear as agglomerates (Fig. 1(b)). A high content of indium in those agglomerates has been detected previously.[15]

Figure 2(a) shows a STM image of an undoped nanorod supported on polycrystalline Au film. The ZnO nanorod with a prismatic geometry (Fig. 2(b)) has surface composed of aligned grains, formed by strain relaxation process as has been reported earlier.[18] Our STS measurements[19] (Fig. 3) on the sample revealed a surface band gap of about 3.5 eV, in agreement with other STS measurements reported for ZnO.[20] Since the Fermi level position corresponds to the zero sample bias, n-type conductivity and donor states at about 1 eV below the conduction band are revealed for the sample.

STM images of the doped nanorods revealed that their surface is composed of grains and aligned nanoparticles of diameters between 4 and 8 nm (Figs. 2(c and d)). From the STS spectra acquired at different locations of the nanorods, we could identify donor and acceptor states, revealed as changes in slope near the conduction and valence bands

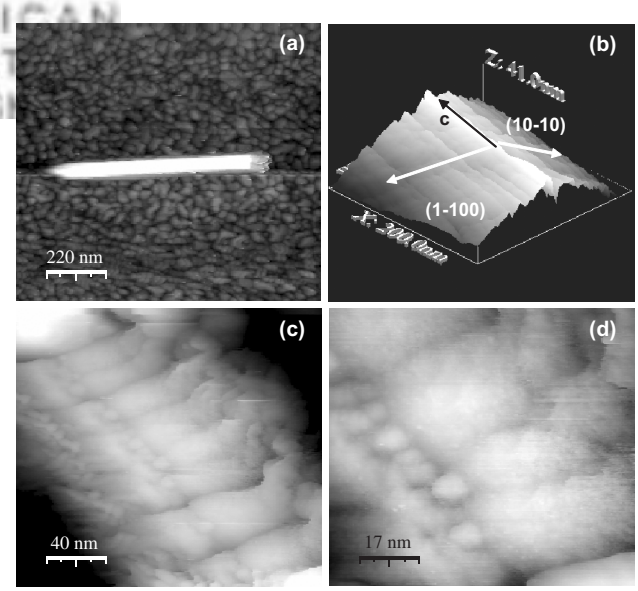

Fig. 2. STM images of (a) an undoped ZnO nanorod supported on a gold film, exhibiting (b) prismatic geometry. (c) and (d) show STM images of In doped ZnO nanorod with aligned nanoparticles and grains at the surface.

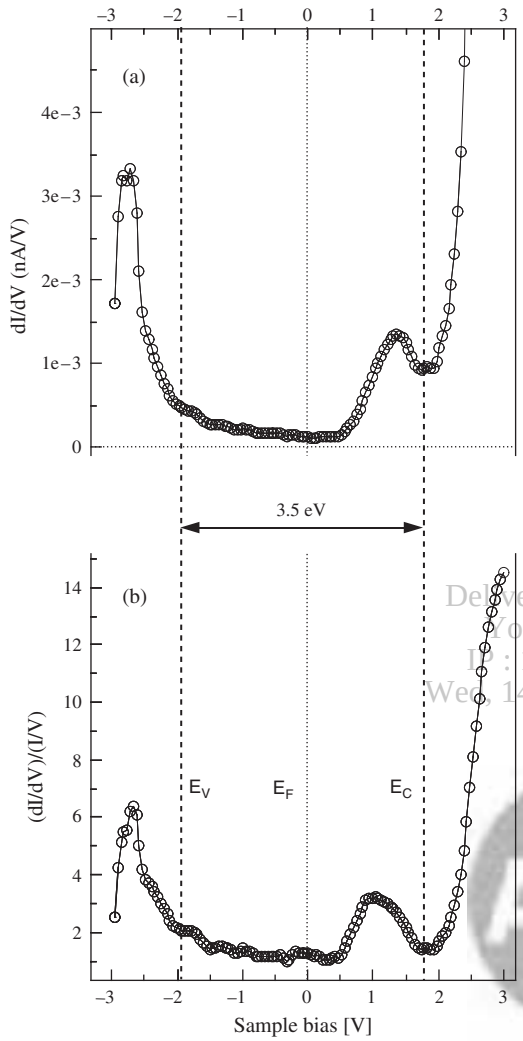

Fig. 3. (a) Differential conductance and (b) normalized differential conductance spectra of undoped ZnO nanorods displaying 3.5 eV energy gap.

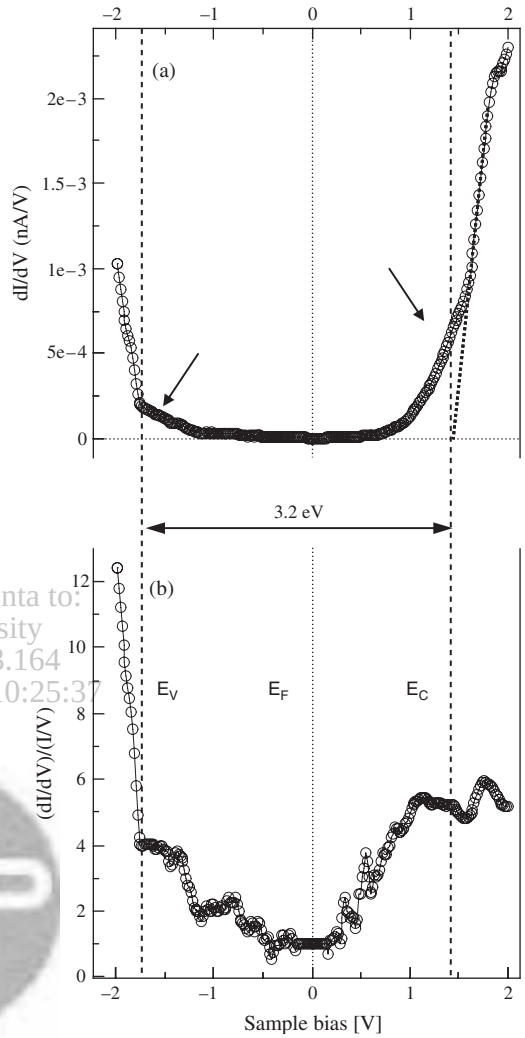

Fig. 4. (a) Differential conductance and (b) normalized differential conductance spectra of the In doped nanorod shown in Figure 2(c), displaying 3.3 eV energy gap.

(arrows in Fig. 4(a)). The conduction band energy was estimated from the differential conductance curve (Fig. 4(a)) as it was not well resolved in the normalized differential conductance spectrum of Figure 4(b). The conduction band for the sample was estimated to be at 1.4 eV above the Fermi level. The surface band gap estimated for this sample was about 3.2 eV. It must be recalled that the band gap value measured through a differential conductance curve can vary with the variation of the separation between the tip and the sample surface. However, we believe that the band gap value we estimated is not very different from the real value as the results were averaged for 5–8 measurements.

High density of grains was found in some In doped ZnO nanorods. In Figure 5(a) such a nanorod with elongated grains of variable sizes is shown. Apparently some of these grains separate easily from the nanorod due to their loose bindings with the main nanorod. Elemental mapping through energy dispersive spectroscopy (EDS) on the nanostructures (not presented) revealed inhomogeneous distribution of indium in them. Moreover, a high concentration of indium was detected in the particles/grains.[15] Figure 5(b) shows a region of the sample composed of grains and nanoparticles, demonstrating morphology modification in ZnO nanostructures by indium incorporation. STS spectra acquired on such nanorods, as presented in Figure 6, revealed high density of acceptor states on the grains. An intense peak was identified at about −0.5 V, that corresponds to 1.26 eV above the valence band. Clearly these acceptors are produced by defects formation in the nanorods evidencing self-compensation of In donor carriers. Through Hall measurements, Oh et al.[22] have demonstrated an inversion of *n*-type to *p*-type conductivity in ZnO films when they were grown at high oxygen pressure. They suggested that the zinc vacancies (V_{Zn}), which act as acceptors in ZnO are responsible for such

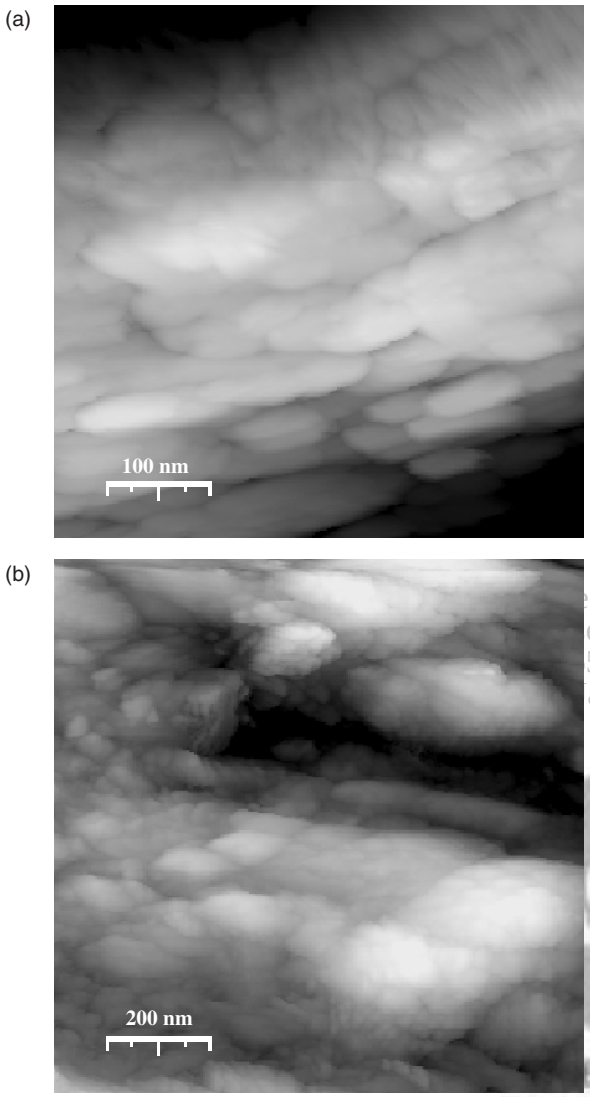

Fig. 5. STM images showing (a) detail of the granular composition of a In doped nanorod, and (b) a region composed of grains and nanoparticles.

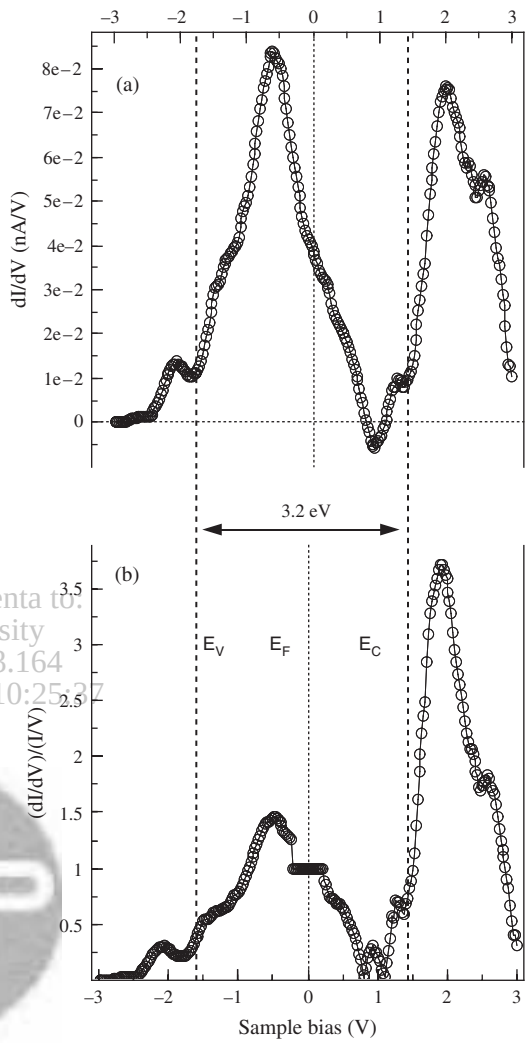

Fig. 6. (a) Differential conductance and (b) normalized differential conductance spectra of a nanorod composed of granular surface similar to the one shown in Figure 5(a).

conductivity inversion effect, as it has the lowest formation energy than other defects.[23] In our previous cathodoluminescence studies of In doped ZnO nanorods, however, we detected the presence of O_i defects in high density.[21] Such an increase of O_i defects in In doped nanorods increases the commonly known yellow and red emissions in them.[24–26] Janotti and Van de Wall[27] have reported zinc vacancies and oxygen interstitial as deep acceptors in ZnO. While the zinc vacancies have transitions $\varepsilon(0/-)$ and $\varepsilon(-/2-)$, at 0.11 and 0.9 eV above the valence band, respectively, the oxygen interstitials have similar transitions at 0.57 and 1.18 eV, respectively. Therefore, we believe, in the indium rich particles or agglomerates on our doped nanostructures, incorporated indium created zinc vacancy sites and probably also V_{zn}-donor impurity complexes. The atomic% of Zn:O:In revealed from the EDS analysis of our doped nanostructures and agglomerates were 46.11:50.78:3.11 and 21.61:58.25:21.14, respectively. Decrease of zinc content in the nanostructures on incorporation of indium also indicates the formation of zinc vacancies in them. The incorporated indium substitute zinc atoms from their lattice sites, creating zinc vacancies, which act as acceptors and can form donor-acceptor pairs doped indium. As in the indium rich agglomerates the zinc content is very low (and indium content very high), lattice distortion and zinc vacancies are very high. Therefore, the effect of donor doping in making the nanostructures more *n*-type is compensated partially. Although the STS measurements at room temperature did not permit us to identify the acceptor energy levels with precision, generation of both acceptor and donor types of defects in the indium doped ZnO nanostructures is revealed clearly.

4. CONCLUSIONS

Indium could be incorporated in ZnO nanostructures through low temperature hydrothermal process and

subsequent thermal annealing in inert atmosphere. Incorporated indium remains inhomogeneously distributed in the nanostructures. High doping concentration of indium induces a drastic morphology change of the ZnO nanostructures, producing lattice defects and zinc vacancies in high concentrations. Apart from the generation of donor states, heavy indium doping creates acceptor states (V_{Zn}) in the nanostructures, which seems to compensate the doped donors to some extent, prohibiting the increase of *n*-type conductivity of the nominally pure ZnO nanostructures. Presence of acceptor states in high concentration in the heavily doped nanostructures could be detected through STS. Creation of acceptor states in nominally *n*-type ZnO by donor incorporation is demonstrated for the first time.

Acknowledgments: Authors are thankful to A. Escobedo Morales for preparing the ZnO nanostructures. The work was supported by CONACyT, México, through the grants # 46269 and # 47505. A. González-Carrazco thanks CONACyT, Mexico for extending the doctoral scholarship.

References and Notes

1. S. Choopun, R. D. Vispute, W. Noch, A. Balsamo, R. P. Sharma, T. Venkatesan, A. Lliadis, and D. C. Look, *Appl. Phys. Lett.* 72, 3947 (**1999**).
2. F. R. Service, *Science* 276, 685 (**1997**).
3. X. Y. Kong and Z. L. Wang, *Nano Lett.* 3, 1625 (**2003**).
4. M. S. Arnold, Ph. Avouris, Z. W. Pan, and Z. L. Wang, *J. Phys. Chem. B* 107, 659 (**2003**).
5. C. Liu, J. A. Zapien, Y. Yao, X. Meng, C. S. Lee, S. Fan, Y. Lifshitz, and S. Y. Lee, *Adv. Mater.* 15, 838 (**2003**).
6. Z. L. W. Pan, Z. R. Dai, and Z. L. Wang, *Science* 291, 1947 (**2001**).
7. X. Wang, C. J. Summers, and Z. L. Wang, *Nano Lett.* 4, 423 (**2004**).
8. W. Lee, M. C. Jeong, and J. M. Myoung, *Nanotechnology* 15, 1141 (**2004**).
9. H. Zhang, X. Ma, J. Xu, J. Niu, and D. Yang, *Nanotechnology* 14, 423 (**2003**).
10. M. J. Zheng, L. D. Zhang, G. G. Li, and W. Z. Shen, *Chem. Phys. Lett.* 363, 123 (**2002**).
11. Ü. Özgür, Ya. I. Alivov, C. Liu, A. Teke, M. A. Reshchikov, S. Doğan, V. Avrutin, S.-J. Cho, and H. Morkoç, *J. Appl. Phys.* 98, 041301 (**2005**).
12. T. V. Butkhuzi, B. E. Tsekvana, N. P. Nekelidze, E. G. Chikoidze, T. G. Khulordava, and M. M. Sharvashidze, *J. Phys. D: Appl. Phys.* 32, 2683 (**1999**).
13. S. Yamauchi, Y. Goto, and T. Hariu, *J. Cryst. Growth* 260, 1 (**2004**).
14. S. A. Studenikin, N. Golego, and M. Cocivera, *J. Appl. Phys.* 84, 2287 (**1998**).
15. A. Escobedo Morales, M. Herrera-Zaldívar, and U. Pal, *Opt. Mater.* 29, 100 (**2006**).
16. J. A. Stroscio, R. M. Feenstra, and A. P. Fein, *Appl. Phys. Lett.* 57, 2579 (**1986**).
17. R. M. Feenstra, J. A. Stroscio, and A. P. Fein, *Surf. Sci.* 181, 295 (**1987**).
18. M. Herrera-Zaldívar, J. Valenzuela-Benavides, and U. Pal. *Opt. Mater.* 27, 1276 (**2005**).
19. MSxM free software downloadable at http://www.nanotec.es.
20. C. Díaz-Guerra and J. Piqueras, *J. Appl. Phys.* 86, 1874 (**1999**).
21. M. Herrera-Zaldivar, J. Valenzuela-Benavides, U. Pal, and A. Escobedo-Morales, *J. Appl. Phys.* (**2006**), submitted.
22. M. S. Oh, S. H. Kim, and T. Y. Seong, *Appl. Phys. Lett.* 87, 0122103 (**2005**).
23. A. F. Morgan, G. Ceder, D. Morgan, and C. G. Van de Walle, *Phys. Rev. B.* 61, 15019 (**2000**).
24. K. L. Wu, G. G. Siu, C. L. Fu, and H. C. Ong, *Appl. Phys. Lett.* 78, 2285 (**2001**).
25. S. Yamauchi, Y. Goto, and T. Hariu, *J. Cryst. Growth* 260, 1 (**2004**).
26. S. A. Studenikin, N. Golego, and M. Cocivera, *J. Appl. Phys.* 84, 2287 (**1998**).
27. A. Janotti and C. G. Van de Walle, *J. Cryst. Growth* 287, 58 (**2006**).

Received: 12 December 2006. Accepted: 28 March 2007.